Original Article

www.jmss.mui.ac.ir

Quantitative Assessment of Retinopathy Using Multi-parameter Image Analysis

Zahra Ghanian[1], Kevin Staniszewski[1], Nasim Jamali[2], Reyhaneh Sepehr[1], Shoujian Wang[2], Christine M. Sorenson[3,4], Nader Sheibani[2,4,5], Mahsa Ranji[1,4]

[1]Biophotonics Laboratory, University of Wisconsin Milwaukee, Department of Electrical Engineering and Computer Science, 3200 N Cramer St., Milwaukee, WI 53211-3029, [2]Departments of Ophthalmology and Visual Sciences, [3]Pediatircs, [4]McPherson Eye research Institute, [5]Biomedical Engineering, University of Wisconsin School of Medicine and Public Health, Madison, WI, 53705-2275, USA

Submission: 19-11-2015 Accepted: 04-04-2016

ABSTRACT

A multi-parameter quantification method was implemented to quantify retinal vascular injuries in microscopic images of clinically relevant eye diseases. This method was applied to wholemount retinal trypsin digest images of diabetic Akita/+, and bcl-2 knocked out mice models. Five unique features of retinal vasculature were extracted to monitor early structural changes and retinopathy, as well as quantifying the disease progression. Our approach was validated through simulations of retinal images. Results showed fewer number of cells (P = 5.1205e-05), greater population ratios of endothelial cells to pericytes (PCs) (P = 5.1772e-04; an indicator of PC loss), higher fractal dimension (P = 8.2202e-05), smaller vessel coverage (P = 1.4214e-05), and greater number of acellular capillaries (P = 7.0414e-04) for diabetic retina as compared to normal retina. Quantification using the present method would be helpful in evaluating physiological and pathological retinopathy in a high-throughput and reproducible manner.

Key words: *Classification, fluorescence microscopy, fractals, image cytometry, retinopathy, segmentation*

INTRODUCTION

Retinopathy involves diverse vascular complexity and other changes in the neuroretina associated with the pathogenesis of many ocular diseases including diabetic retinopathy,[1] hypertension,[2] and age-related macular degeneration.[3] Once the degree of retinopathic injury can be detected, it will be possible to treat and slow down or stop its progression. Therefore, the creation of a system with multi-parameter diagnosis of retinal structural changes in their early stages is a high priority and helpful to investigate the pathogenesis and progression of retinopathy.

Recent studies have reported image procedures on retinopathies.[4-8] However, none of these methods consider more than one feature to classify the retina as either healthy or injured. For example, there are studies using computer-assisted procedures to measure the caliber of retinal blood vessels as a feature of retinopathy,[9-12] and most of these procedures are semi-automatic. In addition, many of these studies analyzed fundus images, which typically lack high resolution. Figure 1 shows a typical mouse fundus fluorescein angiogram image and a mouse retinal vasculature trypsin digest image highlighting the differences between the resolution of these images.

High-resolution microscopy images of the retinal trypsin digest slides allow for quantifying the clinically relevant features of the retinal vasculature, the majority of which cannot be studied in low-resolution fundus images. Wholemount retinal trypsin digest, which is the gold standard method for analyzing the diabetic retinal vasculature,[13,14] makes it possible to study various structural changes such as capillary degeneration, vascular cell apoptosis, and microaneurysms.[15] The first two abnormalities are correlated with changes in retinal vasculature during early stages of diabetes, hypertension,[16] and also are seen in mice with bcl-2 deficiency. The bcl-2 expression plays an important role in

Address for correspondence:
Prof. Mahsa Ranji, University of Wisconsin-Milwaukee, Biophotonics Lab, EE Department, 3200 N Cramer St, EMS room 1195, Milwaukee, WI 53211, Tel: (414) 229-5889, Fax: (414) 229-6958, USA.
E-mail: ranji@uwm.edu

How to cite this article: Ghanian Z, Staniszewski K, Jamali N, Sepehr R, Wang S, Sorenson CM, *et al*. Quantitative Assessment of Retinopathy Using Multi-parameter Image Analysis. J Med Sign Sence 2016;6:71-80.

regulating apoptosis and angiogenesis, and its deficiency is associated with decreased number of vascular cells and vascular density in the retina.[17]

We have developed a multi-parameter image cytometry tool to quantify the parameters associated with the early stages and progression of retinopathic injury during diabetes. Using this tool, two different vascular cell types, endothelial cells (ECs) and pericytes (PC) can be segmented and the number of each cell type quantified and the ratio of EC to PC (EC/PC ratio) calculated. Present tool also determines other retinal vascular parameters including the number of acellular capillaries, vessel coverage, and fractal dimension, all of which correlate with progression of diabetic retinopathy.[18-20] To the best of our knowledge, this is the first time that automatic multi-feature quantification of diabetic retinopathy and vascular changes in retinal trypsin digests has been presented. Our quantification method measures subtle retinal vascular changes, which are markers of early microvascular dysfunction during diabetes. Such developments will open the door for advanced quantitative assessments, which could substantially contribute to a better understanding of the pathogenesis and prediction of diabetic retinopathy. Moreover, our cytometric tool selects two, three, or all of the detected parameters depending on the disease stage, and utilizes classification techniques to separate healthy and injured retina. This tool allows for automated analysis of retinal trypsin digest preparations for high throughput assessment of structural retinopathy changes when needed.

MATERIALS AND METHODS

Animal Models

Retinal vascular parameters are compared in diabetic mice (6 months and 11 months of age) and bcl-2 deficient mice (6 weeks of age) with their corresponding wild types (WTs). Retinal trypsin digests from diabetic Akita/+ mice, bcl-2 deficient (bcl-2−/−) mice, and WT mice were prepared and imaged. Akita/+ mice (Jackson Laboratory, Bar Harbor, ME, USA) have a mutation in their insulin gene, and the heterozygous male (Akita/+) mice become diabetic by 4 weeks of age. The retinas from these mice show differences in cell distribution and vasculature complexity.[21] They also show the growth of acellular capillaries, which are vessels that contain no cell nuclei, with long-term diabetes. These vessels are very thin and are a common hallmark of nonproliferative diabetic retinopathy.

The germline-targeting of the bcl-2 gene and the generation of mutant mice have been previously described.[22] Litters produced by mating heterozygote mutant mice are genotyped by PCR of genomic DNA extracted from tail biopsies. bcl-2−/− mice exhibit decreased retinal vascular density during the development of retinal vasculature prior to 6 weeks of age. Decrease in retinal vascular density is mainly attributed to decreased numbers of ECs and PC in the absence of bcl-2.[17] These studies were conducted in accordance with the ARVO statement for the Use of Animals in Ophthalmic and Vision Research and approved by the Institutional Animal Care and Use Committee of University of Wisconsin School of Medicine and Public Health.

Microscope Slide Preparations

A total of 14 mice were sacrificed including three 6-week-old bcl2−/− and their WT littermates, two 6-month-old diabetic Akita/+ and their WT littermates, two 11-month-old diabetic Akita/+ and their WT littermates. Retinas ($n = 28$) of these six groups of mice were digested in a solution of trypsin, which carefully leaves retinal vascular network intact while digesting other tissues. Following the digestion, retinal vascular preparations are mounted on charged slides, dried, stained with periodic acid-Schiff and hematoxylin, and coverslipped for virtualization and quantitative assessments, as previously described by us.[23]

Microscopy Imaging

The retinal trypsin digests were imaged using an inverted fluorescence microscope (Nikon Ti-E) at a magnification of ×40. The images were captured using a CCD camera (QImaging EXi Aqua) at a resolution of 1392 × 1040 pixels, leading to a scale of approximately 0.16 μm per pixel. Red fluorescence filter set with excitation at 540 nm (25 nm bandwidth) and the emission at 620 nm (60 nm bandwidth) was used. Images obtained under these settings captured the vasculature network of the retina [Figure 1, middle image]. Besides fluorescence imaging, brightfield imaging was performed to capture cell nuclei images [Figure 1, bottom image]. Four fields of view were chosen from each group of retina. The fields of view were chosen from the mid- and far-periphery areas of the retinas, one field of view (FOV) in each quadrant of retina. The acquired images were saved as TIFF files and analyzed in MATLAB (MathWorks, Inc. Massachusetts 01760 USA).

Cell Detection and Count

The image processing program is based on the retinal cell image (bright field) to segment two vascular cell types, EC and PC. The contours of the cell nucleus in each image are determined using the segmentation algorithms shown in Figure 2. The gradient of the cell images was calculated, and the magnitude of this gradient was considered as the segmentation function [Figure 2b, third stage, top image]. To avoid over-segmentation,[24,25] the segmentation function was modified based on the foreground and background markers [Figure 2b, third stage, bottom image]. The location of foreground markers (cells) is detected by applying a spatial finite impulse response (FIR) filter[26] to enhance the object-background contrast[27,28] and simplify the subsequent threshold step.

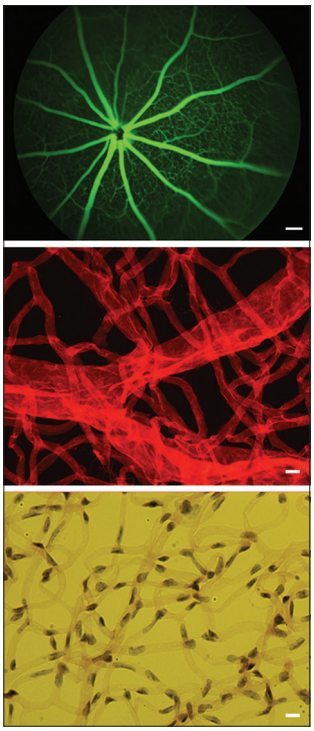

Figure 1: Fundus camera and microscopy images of retina. Top: A fluorescein angiogram of mouse eye using a fundus camera (scale bar represents 100 μm). Middle and Bottom: Microscopy vasculature and cell nuclei images acquired from wholemount retinal trypsin digest used in this study to detect changes in retinal vasculature and vascular cells (scale bar represents 15 μm)

For image $g(x, y)$, class $c(x, y)$, and spatial FIR filter $k(x, y)$, the contrast enhancement procedure is:[26]

$$f(x,y)=k(x,y)^{*}g(x,y)$$
$$C(x,y)=\begin{cases}C_0, f(x,y)<T\\ C_1,\ f(x,y)\geq T\end{cases} \quad (1)$$

where * is the convolution operator, $f(x, y)$ is the filtered image, C_0, and C_1, represent the two classes of the filtered images, and T is the threshold. T was initialized using Otsu method[29] to minimize the weighted sum of the intensity variance within each of the pixel classes (C_0, and C_1). Then using adaptive thresholding,[30] the threshold level for each pixel is optimized based on the intensity statistics of a local neighborhood surrounding the pixel. Function $C(x, y)$, is a two-category linear classifier implemented as a spatial FIR filter. Given an ideal classified image $i_c(x, y)$ and the input image $g(x, y)$, the optimum FIR filter that maps $g(x, y)$ to $i_c(x, y)$ is obtained.[26]

$$e(x,y)=\sum\begin{cases}(i_c(x,y)-f(x,y))^2, A<f(x,y)<B\\ 0, \qquad\qquad \text{otherwise}\end{cases} \quad (2)$$

where error $e(x, y)$ is nonzero only when the filter has not acquired the contrast defined by (A, B). Minimization of $e(x, y)$ results in a filter $k(x, y)$ that yields the best contrast for successive thresholding within (A, B). This filter emphasizes the objects by amplifying intensity of the

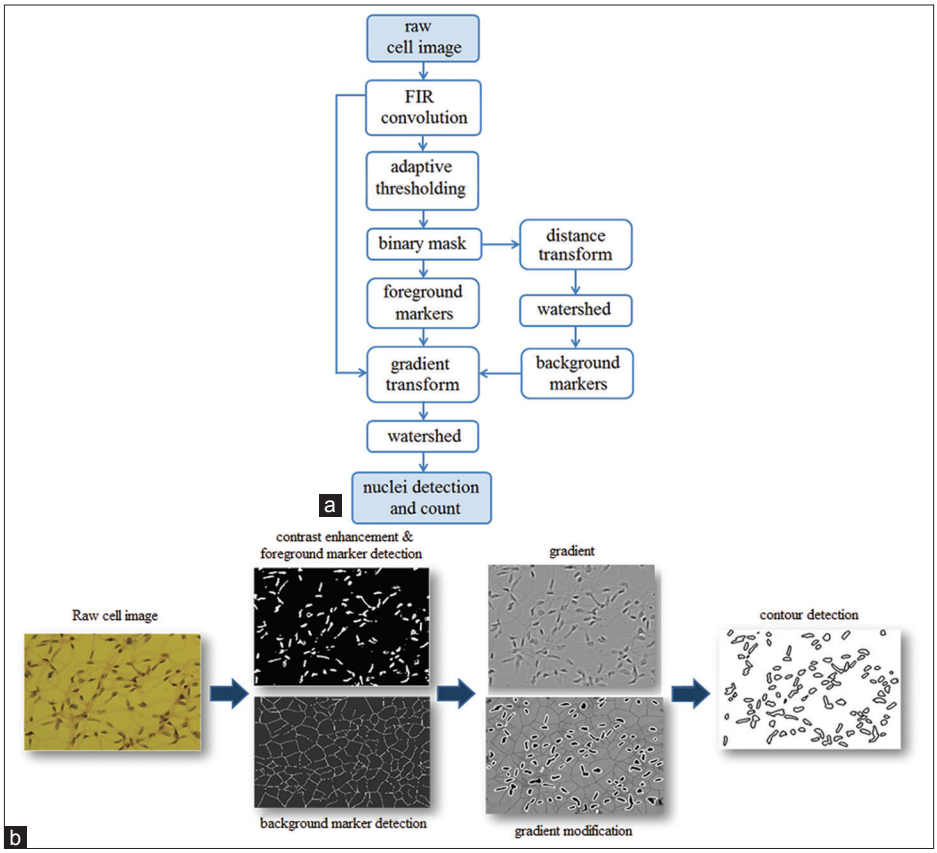

Figure 2: (a) Flowchart of the cell segmentation procedure. (b) Output of the segmentation algorithm in different stages

pixels within the object while negating pixels outside of the objects to create a high foreground-background contrast in the image [Figure 2b, second stage, top image].

With the location of the cells detected by thresholding the filtered image, a distance transform is calculated for the resulting image, in which each pixel value is transformed into the distance to the nearest cell. Background markers are then computed by applying watershed[30] detection on the resultant distance image from the previous stage [Figure 2b, second stage, bottom image]. Using SKIZ method,[31] watershed detection finds the "ridges" in an image, leads to areas where the distance to the nearest cell is maximal. The resulting background markers are the lines that separate the image into individual cells while maintaining the maximum distance between any line and the nearest cell. The segmentation function is then modified so that only its regional minima occur in the foreground and background markers [Figure 2b, third stage, bottom image]. At this stage, the watershed transform[30] of the modified segmentation function was computed which results in a binary mask containing the borders of the cells [Figure 2b, last stage].

Calculation of the Endothelial Cells to Pericytes Population Ratio

Nuclear morphology was used to distinguish between PCs and ECs. PCs have a round nuclei and protuberant position, whereas ECs have a more elliptical shape. Since PC is more round, the ellipticity of the cell is used as a parameter to determine whether a cell is EC or PC. In short, the diameter of the cell was measured for each pixel in the cell border by determining the distance between the pixel and a pixel exactly half way around the border of the cell. The ratio of the largest diameter to the shortest was then stored as the ellipticity of the cell. Cells with ellipticity >2 were categorized as EC, and all other cells were categorized as PC. The threshold value of 2 is found empirically to best correlate with the results of expert analysis.

To evaluate the accuracy of the proposed nuclei segmentation and cell type determination, sixteen FOVs of four retinas from 11-month-old WT mice were considered that covered over 1000 nuclei. Since there is no ground truth for the segmentation, manual evaluation was used as a benchmark, and we compared the automatic approach to this manual benchmark for accuracy counts [Table 1].

Acellular Capillary Detection and Count

The number of acellular capillaries is another parameter of interest. These are also referred to as ghost vessels that are a sign of later nonproliferative complications of diabetes. Acellular capillaries are those blood vessels, which have no cell nuclei and lack perfusion, and as a result have smaller

Table 1: Accuracy of the cell count and cell type determinations for 16 fields of views of images from four 11-month-old wild-type mice

Approaches	EC count	PC count	Cell count	E/P	Cell count accuracy (%)	E/P accuracy (%)
Manual	1161	688	1849	1.69	100	90
Proposed	1071	619	1690	1.73	91.4	87.87

EC: Endothelial cell, PC: Pericyte

widths than healthy capillaries [Figure 3a, white arrow]. The program measures the caliber of the vasculature using binary image [Figure 3b] and marks areas which have a width $<40\%$ of the average width of vessels in the retina [Figure 3d]. Using morphological tools, the connection of the pixels in the marked areas in a small neighborhood was then investigated. Capillaries with a diameter smaller than 20% of adjacent capillaries were identified as strands or touching vessels and were not counted.

To determine the vessel caliber, defined as the average width of vessels, the total area of the vasculature from the original binary image was divided by the total length of the vessel. The total vessel length was determined using the morphologically thinned vasculature. A skeleton-based method[32] was applied to achieve the thinned vasculature image. In this image, the entire vasculature was reduced to a cross-sectional width of 1 pixel [Figure 3c]. Thus, the total number of pixels representing the vasculature is equal to the total length of all vessels within the retina.

The performance of the acellular capillary detection algorithm is dependent on the quality of the binary image containing the retina vasculature and acellular capillaries. This binary image is implemented by dynamic local thresholding. The threshold level was initialized applying mixture models method[33] and then fine-tuned locally for each 32×32 neighborhood within the image to detect very thin acellular capillaries.

Determination of Fractal Dimension

Fractal dimension of the retinal vasculature is another parameter quantified using a technique known as the box-counting method.[34-37] In this method, the vasculature image was first divided into a number of smaller "boxes." Then, the number of boxes which contain part of the vasculature was determined. This process was then repeated with boxes of different sizes. If the structure is in fact fractal, an exponential relation is expected between the box size (ε) and the number of boxes required to cover the entire structure (N). Eq. 3 shows this relationship:[34]

$$N = C\varepsilon^{-D_f} \quad (3)$$

where C is a constant of no consequence in this context and D_f is the fractal dimension of the structure. The fractal dimension is found by solving Eq. 3 to obtain an expression

involving a logarithm with base ε. However, while Eq. 3 will work for a true fractal dimension, physical structures do not exhibit fractal behavior on all scales. Thus, the limit of the Eq. 3 must be taken as the box size approaches zero. To do this effectively, L'Hopital's rule can be used to determine the limit of the equation based on the equation's derivative. The fractal dimension can then be found by determining the slope of the log-log plot of N against ε [Eq. 4]:

$$D_f = -\lim_{\varepsilon \to 0} \log_{\varepsilon}^{N} = \frac{\partial(\log_{\varepsilon}^{N})}{\partial \varepsilon} \quad (4)$$

Vessel Coverage

One of the markers of late-stage retinopathy is a denser vasculature. Total vessel coverage is determined for each FOV by the total number of pixels representing the vasculature in the binary image.

Classification of Retinal Images

The quantified parameters of the cell and vasculature images of the retinas were used to classify retinas as normal or injured. The classification was performed using a nonlinear classifier, support vector machine (SVM). SVM classifier attempts to maximize the margin of error and allows for better generalization of the results.[38] This Kernel-based classifier uses radial basis functions and the kernel trick to project the data into a high dimensional space for easier separation. Gaussian radial basis function was used in the current study to map the training data set into kernel space where a maximal separating hyperplane was constructed.

The accuracy, sensitivity, and specificity of the classification are calculated through the following equations:

$$\text{Accuracy} = \frac{TP + TN}{TP + TN + FP + FN}$$

$$\text{Sensitivity} = \frac{TP}{TP + TN}$$

$$\text{Specificity} = \frac{TN}{TN + FP} \quad (5)$$

where TP and FN are the number of diabetic retinas classified as diabetic or normal, respectively. Similarly, TN and FP are the number of normal retina detected as normal or diabetic. FN and FP were determined using the leave-one-out cross-validation method.[39] In this method, one data point is withheld from the system during its training phase, and then the point is classified using the newly trained system.

Statistical Analysis

Two-tailed Student's *t*-test is used for normally distributed data (n = 16 FOVs for each group). $P < 0.05$ is considered significant.

RESULTS

In this study, we have established an image analysis tool to assess and quantify the structural changes in the retinal vasculature either at the early stage of the disease or as the injury progresses. To determine the effect of diabetes and germline deletion of bcl-2 on the retinal vasculature, five parameters were quantified in retinas from bcl-2−/− mice and their control littermates at 6 weeks of age, as well as retinas from Akita/+ mice and control littermates at 6 and 11 months of age. The results of this method demonstrated a 26.43%, 16.6%, and 25.7% fewer number of cells and 12.38%, 14.97%, and 17.8% lower vessel coverage in the three aforementioned groups of the diseased retina compared to the corresponding controls. Both groups of diabetic retinas at 6 and 11 months of age showed higher EC/PC ratio compared to their controls (38.7% and 33%, respectively) and only 11-month-old diabetic retinas showed significantly larger number of acellular capillaries (126.3%) and higher fractal dimension (1.1%) compared to the control. The details of the results for the 11-month-old diabetic retinas, developing changes in the five features, are provided.

Injured Retinas have Fewer Number of Cells

The retinas from diabetic mice contained fewer cells compared to the WT normal mice of the same age [Figure 4a, left panel]. For instance, the 11-month age group images from mid- and far-periphery areas of retina (16 FOVs) contained a mean number of 78.5 cells in diabetic mice and 105.6 in the WT mice (P = 5.1205e-05). The first two bars in Figure 4b represent the mean and standard errors of the cell counts scaled by 10^{-1} within each group. The higher mean values in the WT groups showed that diabetes caused vascular cell death in the retina. Please note that cell segmentation algorithm resulted in an accuracy of 91.4% compared to manual cell count [Table 1].

Diabetic Eyes have a Higher Endothelial Cell/Pericyte Ratio

One of the hallmarks of early diabetic retinopathy is loss of PC. With progression of the disease, retinal vessels lose PC, leading to vascular dysfunction such as increased permeability and loss of EC. Thus, loss of PC results in a higher EC/PC ratio in diabetic retinas compared with retinas from WT mice. The images showed a mean EC/PC ratio of 2.4053 for diabetic 11-month-old mice and 1.8084 for the WT mice (P = 5.1772e-04). As expected, the mean values were lower in WT groups than those in the diabetic groups. Figure 4b shows the mean and standard errors of the EC/PC ratios within each 11-month-old group. PC determination algorithm resulted in 87.87% accuracy in the EC/PC ratio on average compared to manual evaluation [Table 1].

Diabetic Retinas have a Larger Number of Acellular Capillaries

Acellular capillaries in the retina arise from chronic exposure to hyperglycemia, have no cell nuclei and exhibit a very small width. The results from the vasculature images (from mid- and far-periphery areas of retina) showed a significant difference between the number of acellular capillaries in the WT and Akita/+ 11-month-old mice [Figure 4a, right panel]. The mean acellular capillary number were 2.375 and 5.375 for WT and Akita/+ mice, respectively (P = 7.0414e-04). Figure 4b displays the mean value and standard errors of the number of acellular capillaries.

Injured Retinas have Lower Vessel Coverage

Our results indicated that the total area of the vasculature in the retinas from diseased mice was smaller compared to WT mice [Figure 4a, right panel]. The mean values of the number of pixels representing the vasculature were 672,050 and 817,790 for diabetic and WT nondiabetic 11-month-old mice, respectively (P = 1.4214e-05). Figure 4b shows the mean and standard error of the vasculature area scaled by 10^{-5} for each group.

Diabetic Retinas Exhibit Greater Fractal Dimension

Our studies reveal a difference between the fractal dimensions measured in the retinal images of diabetic and nondiabetic 11-month-old mice. The mean values of the fractal dimension were 1.8733 and 1.8499 for diabetic and nondiabetic mice, respectively (P = 1.9167e-08). Figure 4b shows the mean and standard error of these samples, illustrating a significant difference between the two groups. These results suggest that greater retinal fractal dimension, representing increased geometric complexity of the retinal vasculature as a sign of chronic diabetic retinopathy.

Classification of Retinal Images Resulted in 85% Accuracy

Table 2 provides classification results with different feature combinations. Features were selected based on the type and duration of the disease. Left panel in Figure 5 shows the distribution of two features (cell count and vessel coverage) as an example of the classification using SVM classifiers. Crosses correspond to bcl-2 deficient retinas and stars are related to normal retinas (control). The hyperplane on the top right corner is one of the classifiers that indicate the decision boundary between the two groups. This classification resulted in 85.4% accuracy, 94.8% sensitivity, and 77.5% specificity. The right panel in Figure 5 represents the SVM classifier using three features including cell count, vessel coverage, and EC/PC ratio. The surface between yellow (diabetic) and blue (normal) regions is one of the classifiers, which makes the decision boundary between the two groups. Using these three features yielded in the classification with 85.3% accuracy, 88.8% sensitivity, and 81.7% specificity.

Table 2: Performance of the support vector machine classifier for different groups under study

Disease	Age	Features	Accuracy	Sensitivity	Specificity
Bcl-2 deficiency	6 weeks	Cell count, vessel coverage	85.4	94.8	77.5
Diabetes, Akita/+	6 months	Cell count, vessel coverage, EC/PC	85.3	88.8	81.7
	11 months	Cell count, vessel coverage, EC/PC, acellular capillary count, fractal dimension	75	71.7	81.7

EC: Endothelial cell, PC: Pericyte

DISCUSSION

We have developed a novel multi-parameter quantification method to evaluate the health of retinal vasculature. This method employs image processing algorithms to detect the retinal parameters of interest including vessel coverage, acellular capillary count, fractal dimension, and vascular cell count and cell type. To validate the use of the proposed method, we compared the accuracy of the nuclei segmentation and cell type determinations with manual evaluations. Accuracy counts were divided into two categories: EC counts and PC counts. Based on these two counts, the total cell count and EC/PC ratios were evaluated and shown in Table 1. The total number of nuclei identified by each method was not the same. Overall, nuclei segmentation algorithm resulted in an accuracy of 91.4% compared to manual cell counting. The main source of error in the cell count was under-segmentation problem occurred due to overlapping cell nuclei. Segmentation of images containing touching and overlapping cell nuclei is a challenge in cell segmentation,[40,41] and further investigation is needed to further reduce this error. New segmentation methods, including region-based active contour[42,43] (single phase and multiphase), and graph cut-based active contour[44] were also examined. None of these methods were able to improve the segmentation accuracy for our application. Therefore, marker-based segmentation method was chosen for high throughput applicability.

It should also be noted that EC counts and PC counts assessed by each method were not the same. For computer-based approach, the most common error is the under-segmentation, while for manual segmentation, the discrepancy on whether to identify certain nuclei as EC or PC play a much larger role in accuracy rate. The inconsistency between the manual evaluations of cell type provides an idea of how well one could expect to do in comparison to the chosen standard. If two experienced biologists can only

agree on 90% of the cell type results, then it is likely that any claim of above 90% for automatic cell type detection is just accidental. Our results suggest that performance of the proposed method for determining the cell type is comparable to manual evaluation. Considering the manual segmentation accuracy of around 90%, which is only 2.13% better than automatic segmentation method; our results reflect the overall difficulty of the problem and indicate good performance for the automatic method.

The presented multi-parameter quantification method can analyze and monitor vasculature complexity in rodent models of diabetic retinopathy and bcl-2 deficiency. Cell apoptosis,[45-49] loss of PC,[50-54] and lower vessel coverage are used to assess early signs of nonproliferative diabetic retinopathy. However, increased number of acellular capillaries[20,52] and higher fractal dimension[55-58] were later

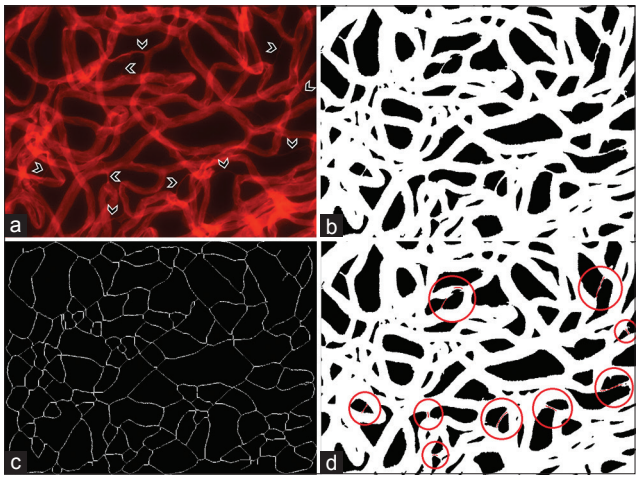

Figure 3: Acellular capillary detection: (a) vasculature image (b) binary image of vasculature (c) morphological thinning of vasculature used to determine vessel caliber (d) marked connected areas with a width <40% of the average vessel's caliber

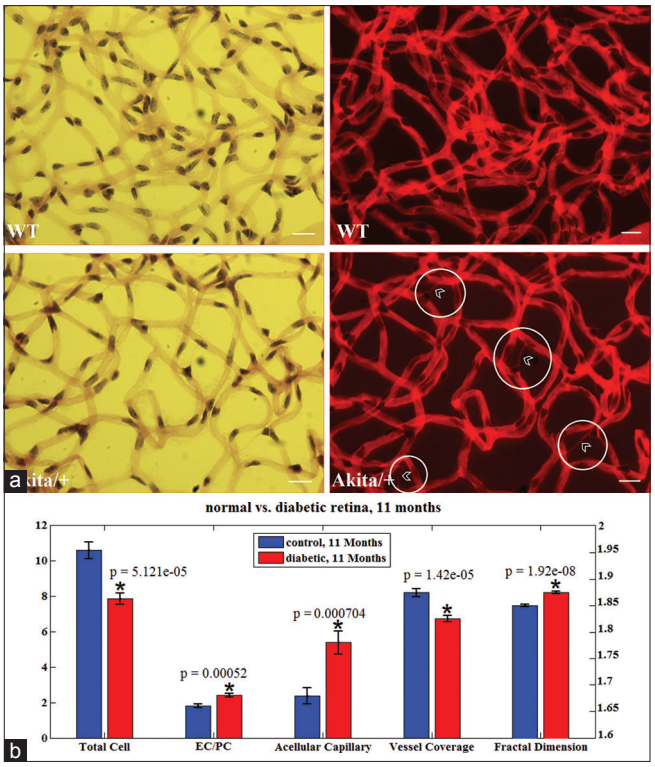

Figure 4: (a) Left: cell images represent that 11-month-old diabetic retina has a fewer number of cell compared to the normal retina at the same age. Right: vasculature images demonstrate lower vessel coverage and larger number of acellular capillaries (shown by arrows) in diabetic retina as compared to control (scale bars represent 20 μm). (b) Bar graph plot comparing five unique features in diabetic retina versus normal retina from 11-month-old mice. Bar graphs show the mean values and standard errors of each feature detected in retinas. Diabetic retinopathy resulted in significant decrease statistically in the total number of vascular cells, and vessel coverage while increase significantly the EC/PC ratio, number of acellular capillaries and fractal dimension. Please note that the total number of cells and vessel coverage were scaled by 10^{-1} and 10^{-5}, respectively. For showing the difference between the fractal dimensions of the two groups, this parameter was presented with different y-axis on the right. The number of the fields of view in each group of retina is 16

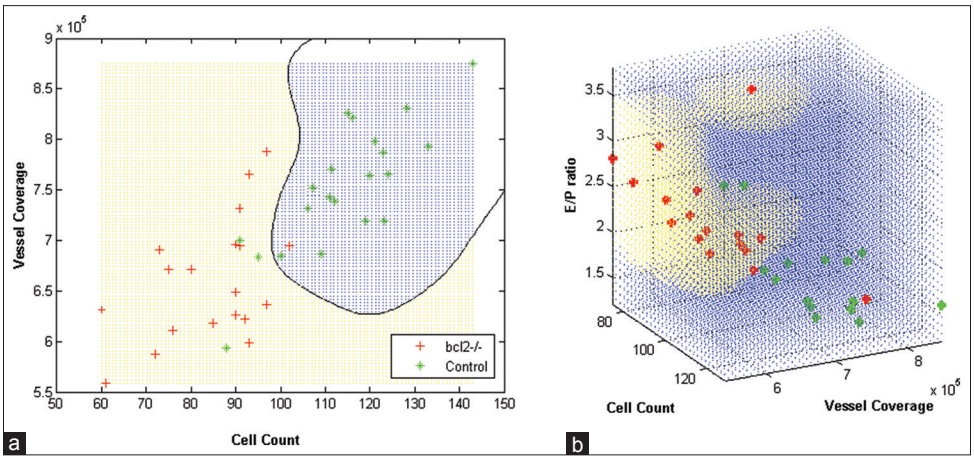

Figure 5: Results of the classification using support vector machine method in retinas from (a) 6 weeks bcl-2−/− deficient and WT mice considering two features: Cell count and vessel coverage (b) 6 months diabetic Akita/+ and WT mice with three features: Cell count, vessel coverage, and EC/PC ratio; Red crosses correspond to injured retinas and green stars are related to control. The boundary between yellow (injured) and blue (normal) regions is one of the classifiers

complications and become more numerous with progression of diabetes. Diabetic retinopathy is a progressive disease and goes through all of these changes in a timely manner. Loss of PC is an early event, which is followed by vascular dysfunction, loss of EC, formation of acellular capillaries and microaneurysms, ischemia, and ultimately neovascularization that is the latest stage of the disease and is normally not seen in rodents. Our multi-parameter method selects these features based on the duration of diabetes as a significantly dominant marker for detection of diabetic retinopathy. The duration of diabetes has a significant impact on the parameters indicated above. Thus, for animals with the longest duration of diabetes, all these changes are significant marker of diabetic retinopathy. Therefore, with longer duration of diabetes in 11-month-old groups all the features can be used to quantify the retinal changes and train the classifier. Figure 4 demonstrates that 11-month-old diabetic retinas have a lower cell density and vessel coverage but a greater EC/PC ratio, higher number of acellular capillaries, and larger fractal dimension.

The fractal dimension, which is a useful measure of the complexity present in the retinal vasculature, determines the self-similarity of the vessel structure. As retinopathy progresses, new and smaller blood vessels begin to grow out of the existing larger vessels, with similar characteristics to the larger vessels, showing that the vessel structure is in fact fractal. Our measured fractal dimension is close to the reported fractal dimension of a diffusion-limited aggregation process (~1.7).[55-58] In addition, there is a correlation between retinal complexity and fractal dimension. This correlation occurs because of the properties of fractal dimensions, which increases as the new vessels grow in with the same properties as the existing larger vessels. Our studies showed that greater retinal fractal dimension represents increased geometric complexity of the retinal vasculature associated with diabetic retinopathy. Since significant increases in acellular capillary formation and fractal dimension are usually observed after 6 months of diabetes,[46,52,59] these parameters are not appropriate to quantify injury in the 6 month-old diabetic groups. Thus, only cell count, vessel coverage, and EC/PC ratios were used for classification [Figure 5b].

In addition to diabetic retinopathy, another type of retinopathy induced by bcl-2 deficiency was studied. Vascular cell count and retinal vascular density were selected as the markers for the early diagnosis of this type of retinopathy.[17] The cell count is an important indicator of retinopathy, as it is directly related to the early loss and later growth of new blood vessels. Thus, we expect the concentration of vascular cells in the retina and also vascular density to be two precursors of retinopathic injury at the early stages. At 6 weeks of age, bcl-2−/− and healthy retinas were classified [Figure 5a] with 85% accuracy showing that these two features are significantly effective, and our multi-parameter method is sensitive to quantify the early structural changes of retina with bcl-2 deficiency.

CONCLUSION

We have studied morphological details of retina including cell count, vessel coverage, and the EC/PC ratios which were associated with loss of the PC as the earliest sign of diabetic retinopathy.[53] Other quantifiable morphological features such as acellular capillaries and fractal dimension correlated with progression of diabetic retinopathy,[56] were also investigated. The current multi-feature method has the capability to detect and quantify the structural changes in the vasculature of retina at the early stages of the disease and provides an opportunity to get a comprehensive view of retinal vasculature at the cellular level. Therefore, with new advancements in new imaging modalities with cellular resolution, it will be possible to utilize the method developed here for quantitative evaluation of retinal vasculature with significant accuracy. This knowledge will be instrumental in development of new treatment modality to stop the development and progression of the disease and save vision. With the addition of more features, we hope to create a system capable of detecting and classifying even small changes in the retinal vasculature, allowing for the earliest detection of the injury. Our system can also be used to assess the impact of various gene mutations, deletions, and overexpression on retinal vascular development and function in a high-throughput and reproducible manner.

Financial Support and Sponsorship

This work was supported in part by UWM RGI 8, UWM UW Madison intercampus grant (MR), RC4 EY021357, P30 EY016665, R21 EY023024, R24 EY022883, Retina Research Foundation, and an unrestricted departmental award from Research to Prevent Blindness. NS is a recipient of research Award from American Diabetes Association, 1-10-B-160 and Retina Research Foundation. CMS is a recipient of Retina Research Foundation-Daniel M. Albert Chair.

Conflicts of Interest

There are no conflicts of interest.

REFERENCES

1. Klein R, Klein BE, Moss SE, Davis MD, DeMets DL. The Wisconsin epidemiologic study of diabetic retinopathy. II. Prevalence and risk of diabetic retinopathy when age at diagnosis is less than 30 years. Arch Ophthalmol 1984;102:520-6.
2. Wong TY, Mitchell P. Hypertensive retinopathy. N Engl J Med 2004;351:2310-7.
3. Bressler NM, Bressler SB, Fine SL. Age-related macular degeneration. Surv Ophthalmol 1988;32:375-413.
4. Wittenberg LA, Jonsson NJ, Chan RV, Chiang MF. Computer-based image analysis for plus disease diagnosis in retinopathy of prematurity.

J Pediatr Ophthalmol Strabismus 2012;49:11-9.
5. Ikram MK, Cheung CY, Lorenzi M, Klein R, Jones TL, Wong TY; NIH/JDRF Workshop on Retinal Biomarker for Diabetes Group. Retinal vascular caliber as a biomarker for diabetes microvascular complications. Diabetes Care 2013;36:750-9.
6. Thomas GN, Ong SY, Tham YC, Hsu W, Lee ML, Lau QP, *et al.* Measurement of macular fractal dimension using a computer-assisted program. Invest Ophthalmol Vis Sci 2014;55:2237-43.
7. Abràmoff MD, Folk JC, Han DP, Walker JD, Williams DF, Russell SR, *et al.* Automated analysis of retinal images for detection of referable diabetic retinopathy. JAMA Ophthalmol 2013;131:351-7.
8. Rasta SH, Partovi ME, Seyedarabi H, Javadzadeh A. A comparative study on preprocessing techniques in diabetic retinopathy retinal images: Illumination correction and contrast enhancement. J Med Signals Sens 2015;5:40-8.
9. Wong TY, Knudtson MD, Klein R, Klein BE, Meuer SM, Hubbard LD. Computer-assisted measurement of retinal vessel diameters in the Beaver Dam Eye Study: Methodology, correlation between eyes, and effect of refractive errors. Ophthalmology 2004;111:1183-90.
10. Li H, Hsu W, Lee ML, Wong TY. Automatic grading of retinal vessel caliber. IEEE Trans Biomed Eng 2005;52:1352-5.
11. Benavent X, Martínez-Costa L, Ayala G, Domingo J, Marco P. Semi-automated evaluation tool for retinal vasculopathy. Comput Methods Programs Biomed 2009;95:288-99.
12. Mahal S, Strain WD, Martinez-Perez ME, Thom SA, Chaturvedi N, Hughes AD. Comparison of the retinal microvasculature in European and African-Caribbean people with diabetes. Clin Sci (Lond) 2009;117:229-36.
13. Bell WR, Green WR, Goldberg MF. Histopathologic and trypsin digestion studies of the retina in incontinentia pigmenti. Ophthalmology 2008;115:893-7.
14. Danis RP, Wallow IH. HRP/trypsin technique for studies of the retinal vasculature. Invest Ophthalmol Vis Sci 1986;27:434-7.
15. Chou JC, Rollins SD, Fawzi AA. Trypsin digest protocol to analyze the retinal vasculature of a mouse model. J Vis Exp 2013;76:e50489.
16. Mohamed IN, Soliman SA, Alhusban A, Matragoon S, Pillai BA, Elmarkaby AA, *et al.* Diabetes exacerbates retinal oxidative stress, inflammation, and microvascular degeneration in spontaneously hypertensive rats. Mol Vis 2012;18:1457-66.
17. Wang SJ, Sorenson CM, Sheibani N. Attenuation of retinal vascular development and neovascularization during oxygen-induced ischemic retinopathy in Bcl-2-/-mice. Dev Biol 2005;279:205-19.
18. Joussen AM, Murata T, Tsujikawa A, Kirchhof B, Bursell SE, Adamis AP. Leukocyte-mediated endothelial cell injury and death in the diabetic retina. Am J Pathol 2001;158:147-52.
19. Klein R, Klein BE, Moss SE, Wong TY, Hubbard L, Cruickshanks KJ, *et al.* The relation of retinal vessel caliber to the incidence and progression of diabetic retinopathy: XIX: The Wisconsin epidemiologic study of diabetic retinopathy. Arch Ophthalmol 2004;122:76-83.
20. Kern TS, Tang J, Berkowitz BA. Validation of structural and functional lesions of diabetic retinopathy in mice. Mol Vis 2010;16:2121-31.
21. Sorenson CM, Wang S, Gendron R, Paradis H, Sheibani N. Thrombospondin-1 deficiency exacerbates the pathogenesis of diabetic retinopathy. J Diabetes Metab 2013; Suppl 12:S12-005.
22. Veis DJ, Sorenson CM, Shutter JR, Korsmeyer SJ. Bcl-2-deficient mice demonstrate fulminant lymphoid apoptosis, polycystic kidneys, and hypopigmented hair. Cell 1993;75:229-40.
23. Wang S, Wu Z, Sorenson CM, Lawler J, Sheibani N. Thrombospondin-1-deficient mice exhibit increased vascular density during retinal vascular development and are less sensitive to hyperoxia-mediated vessel obliteration. Dev Dyn 2003;228:630-42.
24. Arslan S, Ersahin T, Cetin-Atalay R, Gunduz-Demir C. Attributed relational graphs for cell nucleus segmentation in fluorescence microscopy images. IEEE Trans Med Imaging 2013;32:1121-31.
25. Craciunescu T, Murari A, Sieglin B, Matthews G, Contributors JE. An original method for spot detection and analysis for large surveys of videos in JET. IEEE Trans Plasma Sci 2014;42:1358-66.
26. Price JH, Hunter EA, Gough DA. Accuracy of least squares designed spatial FIR filters for segmentation of images of fluorescence stained cell nuclei. Cytometry 1996;25:303-16.
27. Staniszewski K, Sepehr R, Sorenson CM, Sheibani N, Ranji M. Classification of Retinopathic Injury Using Image Cytometry and Vasculature Complexity. In SPIE Proceeding; 2012. p. 822521-822526.
28. Ghanian Z, Staniszewski K, Sorenson CM, Sheibani N, Ranji M. Cytometric Analysis of Retinopathies in Retinal Trypsin Digests. In SPIE Proceeding; 2014.
29. Otsu N. A threshold selection method from gray-level histograms. IEEE Trans Syst Man Cybern 1979;9:62-6.
30. Meyer F, Beucher S. Morphological segmentation. J Vis Commun Image Represent 1990;1:21-46.
31. Preteux E. Watershed and skeleton by influence zones: A distance-based approach. J Math Imaging Vis 1992;1:239-55.
32. Lam L, Lee SW, Suen CY. Thinning methodologies – A comprehensive survey. IEEE Trans Pattern Anal Mach Intell 1992;14:869-85.
33. Huang ZK, Chau KW. A new image thresholding method based on Gaussian mixture model. Appl Math Comput 2008;205:899-907.
34. Kirkby MJ. The fractal geometry of nature. In: Mandelbrot BB, editor. W. H. Freeman and co., San Francisco, (John Wiley & Sons, Ltd; 1983.
35. Bittner H, Wlczek P, Sernetz M. Characterization of fractal biological objects by image analysis. Acta Stereol 1989;8:31-40.
36. Sarkar N, Chaudhuri BB. An efficient differential box-counting approach to compute fractal dimension of image. IEEE Trans Syst Man Cybern 1994;24:115-20.
37. Mandelbrot B. An original method for spot detection and analysis for large surveys of videos in JET. Am Assoc Adv Sci 1967;156:636-8.
38. Cortes C, Vapnik V. Support-vector networks. Mach Learn 1995;20:273-97.
39. Kohavi R. A Study of Cross-Validation and Bootstrap for Accuracy Estimation and Model Selection. In International Joint Conference on Articial Intelligence (IJCAI). San Mateo, CA: Morgan Kaufmann; 1995. p. 1137-43.
40. Coelho LP, Shariff A, Murphy RF. Nuclear segmentation in microscope cell images: A hand-segmented dataset and comparison of algorithms. Proc IEEE Int Symp Biomed Imaging 2009;5193098:518-21.
41. Al-Kofahi Y, Lassoued W, Lee W, Roysam B. Improved automatic detection and segmentation of cell nuclei in histopathology images. IEEE Trans Biomed Eng 2010;57:841-52.
42. Chan TF, Vese LA. Active contours without edges. IEEE Trans Image Process 2001;10:266-77.
43. Vese LA, Chan TF. A multiphase level set framework for image segmentation using the Mumford and Shah model. Int J Comput Vis 2002;50:271-93.
44. Chen C, Li H, Zhou X, Wong ST. Constraint factor graph cut-based active contour method for automated cellular image segmentation in RNAi screening. J Microsc 2008;230(Pt 2):177-91.
45. Engerman RL, Kern TS. Retinopathy in animal models of diabetes. Diabetes Metab Rev 1995;11:109-20.
46. Mizutani M, Kern TS, Lorenzi M. Accelerated death of retinal microvascular cells in human and experimental diabetic retinopathy. J Clin Invest 1996;97:2883-90.
47. Sugiyama T, Kobayashi M, Kawamura H, Li Q, Puro DG. Enhancement of P2X (7)-induced pore formation and apoptosis: An early effect of diabetes on the retinal microvasculature. Invest Ophthalmol Vis Sci 2004;45:1026-32.
48. Kern TS, Tang J, Mizutani M, Kowluru RA, Nagaraj RH, Romeo G, *et al.* Response of capillary cell death to aminoguanidine predicts the development of retinopathy: Comparison of diabetes and galactosemia. Invest Ophthalmol Vis Sci 2000;41:3972-8.

49. Joussen AM, Poulaki V, Mitsiades N, Cai WY, Suzuma I, Pak J, *et al.* Suppression of Fas-FasL-induced endothelial cell apoptosis prevents diabetic blood-retinal barrier breakdown in a model of streptozotocin-induced diabetes. FASEB J 2003;17:76-8.
50. Shimizu K, Kobayashi Y, Muraoka K. Midperipheral fundus involvement in diabetic retinopathy. Ophthalmology 1981;88:601-12.
51. Barber AJ, Antonetti DA, Kern TS, Reiter CE, Soans RS, Krady JK, *et al.* The Ins2Akita mouse as a model of early retinal complications in diabetes. Invest Ophthalmol Vis Sci 2005;46:2210-8.
52. Feit-Leichman RA, Kinouchi R, Takeda M, Fan Z, Mohr S, Kern TS, *et al.* Vascular damage in a mouse model of diabetic retinopathy: Relation to neuronal and glial changes. Invest Ophthalmol Vis Sci 2005;46:4281-7.
53. Midena E, Segato T, Radin S, di Giorgio G, Meneghini F, Piermarocchi S, *et al.* Studies on the retina of the diabetic db/db mouse. I. Endothelial cell-pericyte ratio. Ophthalmic Res 1989;21:106-11.
54. Li W, Yanoff M, Liu X, Ye X. Retinal capillary pericyte apoptosis in early human diabetic retinopathy. Chin Med J (Engl) 1997;110:659-63.
55. Family F, Masters BR, Platt DE. Fractal pattern-formation in human retinal-vessels. Physica D 1989;38:98-103.
56. Cheung N, Donaghue KC, Liew G, Rogers SL, Wang JJ, Lim SW, *et al.* Quantitative assessment of early diabetic retinopathy using fractal analysis. Diabetes Care 2009;32:106-10.
57. Lim SW, Cheung N, Wang JJ, Donaghue KC, Liew G, Islam FM, *et al.* Retinal vascular fractal dimension and risk of early diabetic retinopathy: A prospective study of children and adolescents with type 1 diabetes. Diabetes Care 2009;32:2081-3.
58. Kunicki AC, Oliveira AJ, Mendonça MB, Barbosa CT, Nogueira RA. Can the fractal dimension be applied for the early diagnosis of non-proliferative diabetic retinopathy? Braz J Med Biol Res 2009;42:930-4.
59. Kanwar M, Chan PS, Kern TS, Kowluru RA. Oxidative damage in the retinal mitochondria of diabetic mice: Possible protection by superoxide dismutase. Invest Ophthalmol Vis Sci 2007;48:3805-11.